

Conservation of torus-knot angular momentum in high-order harmonic generation

Emilio Pisanty,¹ Laura Rego,² Julio San Román,² Antonio Picón,^{1,3} Kevin M. Dorney,⁴ Henry C. Kapteyn,⁴ Margaret M. Murnane,⁴ Luis Plaja,² Maciej Lewenstein,^{1,5} and Carlos Hernández-García²

¹*ICFO – Institut de Ciències Fotoniques, The Barcelona Institute of Science and Technology, 08860 Castelldefels (Barcelona)*

²*Grupo de Investigación en Aplicaciones del Láser y Fotónica,*

Departamento de Física Aplicada, University of Salamanca, E-37008, Salamanca, Spain.

³*Departamento de Química, Universidad Autónoma de Madrid, 28049, Madrid, Spain*

⁴*JILA, Department of Physics, University of Colorado Boulder, Boulder, Colorado, 80309, USA*

⁵*ICREA, Passeig de Lluís Companys, 23, 08010 Barcelona, Spain*

(Dated: October 16, 2018)

High-order harmonic generation stands as a unique nonlinear optical up-conversion process, mediated by a laser-driven electron recollision mechanism, which has been shown to conserve energy, momentum, and spin and orbital angular momentum. Here we present theoretical simulations which demonstrate that this process also conserves a mixture of the latter, the torus-knot angular momentum J_γ , by producing high-order harmonics with driving pulses that are invariant under coordinated rotations. We demonstrate that the charge J_γ of the emitted harmonics scales linearly with the harmonic order, and that this conservation law is imprinted onto the polarization distribution of the emitted spiral of attosecond pulses. We also demonstrate how the nonperturbative physics of high-order harmonic generation affect the torus-knot angular momentum of the harmonics, and we show that this configuration harnesses the spin selection rules to channel the full yield of each harmonic into a single mode of controllable orbital angular momentum.

Nonlinear optical processes offer the unique possibility of mediating interactions between modes of the electromagnetic field at different frequencies, transferring energy from one mode to another or to its harmonics [1]. When this transfer happens in a symmetric medium, the interaction will also carry the symmetry’s conserved charge to the recipient mode [2, 3]: in this way, for example, one can combine two photons with well-defined orbital angular momentum (OAM) [4] to make a single photon at twice the frequency and twice the angular momentum [5]. The few-photon exchanges of perturbative nonlinear optics, however, have a relatively limited scale and complexity in comparison to high-order harmonic generation (HHG) [6, 7], where strong-field interactions can produce harmonics with photon energy hundreds or thousands of times larger than the near- or mid-infrared laser driver [8], reaching the extreme-ultraviolet (XUV) or soft x-ray regimes. HHG is a non-perturbative phenomenon for which no first-principles perturbative photon-exchange model is known; instead, it is best understood using a semiclassical picture in which an ionized electron is accelerated back to its parent ion by the laser driver, emitting high-frequency light in the ensuing recollision [9–11]. However, despite the lack of a photon-exchange model, HHG is often regarded as a parametric process, and its conservation properties have been explored extensively as regards energy [12], linear momentum [13], and orbital and spin angular momentum (SAM) [14–21, 22–26].

The individual symmetries associated with these conservation laws of the electromagnetic field can be composed in nontrivial ways to make new ones. This is the case for *coordinated* rotations (CRs): symmetry transformations in which the spatial dependence of the field is rotated by an angle θ about the propagation axis, while the light’s polarization is rotated by $\gamma\theta$ around the same axis, γ being a coordination parameter. CRs are generated by the linear combination $J_\gamma = L + \gamma S$ of the orbital and spin angular momenta, L and S , which

are otherwise independently conserved in the paraxial regime [27]. For monochromatic light, γ is restricted to integer or half-integer values [28, 29], with the latter case imparting on the field the topology of a Möbius strip [30–32]. However, when the monochromatic restriction is lifted, γ can take arbitrary values and still admit invariant states of the field [33], since polychromatic combinations can have polarization states with higher-order internal rotational symmetries.

One particularly relevant example is the three-fold-symmetric trefoil field present in the ‘bicircular’ HHG configurations [22–26, 34–40] used to produce circularly-polarized harmonics. This field consists of two counter-rotating circularly-polarized drivers at different frequencies, and exhibits the same configuration after a polarization rotation by an angle $2\pi/n$, with $n \geq 3$. If we then add different OAM to the two drivers, this polarization rotation can be realized over a 2π rotation of the spatial dependence. The resulting field, which carries both SAM and OAM, but is not an eigenstate of either, has the topology of a torus knot: when the polarization and spatial dependences of the field are unfolded, the trefoil tips trace out a knotted curve embedded on the surface of a torus [33]. With suitable choices of the OAM of the two components, as well as their frequencies (and thus the internal symmetry of the polarization), any arbitrary torus knot [41] can be achieved. Moreover, this topology mirrors the subgroup of the independent-rotations group $\text{SO}(2) \times \text{SO}(2)$ generated by the torus-knot angular momentum (TKAM) $J_\gamma = L + \gamma S$ [33].

In this work, we show that the topological charge J_γ is conserved in high-order harmonic generation for any arbitrary rational coordination parameter $\gamma \in \mathbb{Q}$ [42], providing an infinite family of topological charges (corresponding to an infinite family of dynamical symmetries) that are preserved by the nonperturbative nonlinear interaction. We show that this spin-orbit linking appears in the time domain as a structured spiral of attosecond pulses, and also opens a new window for the exploration

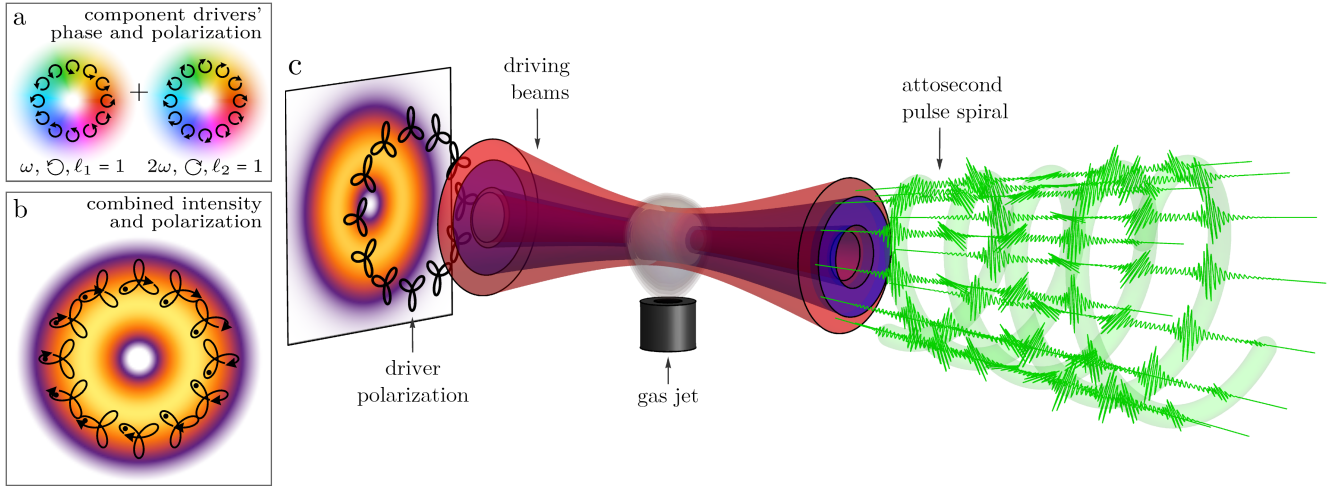


FIG. 1. High-harmonic generation driven by a torus-knot beam. The combination of counter-rotating circular beams at frequencies ω and 2ω with different OAM and therefore different azimuthal phase gradients ((a), with optical phase as the hue color scale) produces a bicircular trefoil polarization which rotates and acquires a delay over azimuthal displacements (b). Here, with $\ell_1 = \ell_2 = 1$, tracking one lobe over an azimuthal loop around the beam axis (black dots) produces a 120° rotation, which induces the topology of a torus knot [33], as well as a time delay within each trefoil (arrows). When this combination incides on a gas jet at high intensity (c), the attosecond pulse trains produced share the coordinated-rotation invariance of the driver, so that the emission at different azimuthal points is related by a time delay and a rotation of the polarization.

of non-perturbative effects in harmonic generation, providing an XUV light source with controllable OAM.

To demonstrate this conservation property, we study HHG driven by TKAM beams that are invariant under coordinated rotations with a mixing parameter $\gamma \in \frac{1}{3}\mathbb{Z}$. This configuration corresponds to a bicircular field consisting of two beams at frequencies ω and 2ω , with counter-rotating right- and left-handed circular polarizations, \textcirclearrowleft and \textcirclearrowright , and carrying independent OAM, ℓ_1 and ℓ_2 , respectively, as shown in Fig. 1. The OAM of the drivers determines the mixing parameter γ under which the bicircular beam is CR-invariant, so that the two components carry TKAM $j_\gamma^{(1)}$ and $j_\gamma^{(2)} = 2j_\gamma^{(1)}$, respectively, which corresponds to identical CR dynamical symmetry for both components. Within that framework, then, the TKAM conservation is expressed as

$$j_\gamma^{(q)} = q j_\gamma^{(1)}, \quad (1)$$

i.e. in the linear scaling of the J_γ charge carried by the q^{th} harmonic with the harmonic order q .

In this configuration, the local field at each point in the beam is the usual bicircular trefoil [22], so that each atom in the target emits harmonics in circularly-polarized doublets with opposite helicities: \textcirclearrowleft -polarized harmonics at harmonic orders of the form $3n+1$, and \textcirclearrowright -polarized harmonics at orders $3n-1$; in the time domain, the emission forms a train of attosecond pulses with linear polarizations at 120° from each other [35, 38]. The orientation of this local trefoil, however, depends on the relative phase between the two components, and, because of the difference in OAM, this phase changes from point to point azimuthally around the beam, so the driver-field trefoil rotates with it, as shown in Fig. 1(b).

The driving field \mathbf{F} does not have any dynamical symmetry that is exclusive to its spatial or polarization aspects: instead, it is invariant only under a coordinated

rotation of the form

$$R(\gamma\alpha)\mathbf{F}(R^{-1}(\alpha)\mathbf{r}, t) = \mathbf{F}(\mathbf{r}, t + \tau\alpha), \quad (2)$$

where τ is a time-delay constant, and the angle α parametrizes the transformation. Here the rotations act on the circular polarization basis $\hat{\mathbf{e}}_\pm = \frac{1}{\sqrt{2}}(\hat{\mathbf{e}}_x \pm i\hat{\mathbf{e}}_y)$ and on the spatial dependence via

$$R(\gamma\alpha)\hat{\mathbf{e}}_\pm = e^{\mp i\gamma\alpha}\hat{\mathbf{e}}_\pm \quad (3a)$$

$$R^{-1}(\alpha)(r, \theta, z) = (r, \theta - \alpha, z), \quad (3b)$$

i.e. as an active and a passive transformation, respectively, with the polarization rotation $R(\gamma\alpha)$ acting through a fraction $\gamma\alpha$ of the spatial rotation angle α .

Our driving field consists of two components with well-defined SAM and OAM,

$$\mathbf{F}_1(\mathbf{r}, t) = \text{Re} [F_1 \hat{\mathbf{e}}_+ f_1(r, z) e^{i\ell_1 \theta} e^{-i\omega t}] \quad (4a)$$

$$\mathbf{F}_2(\mathbf{r}, t) = \text{Re} [F_2 \hat{\mathbf{e}}_- f_2(r, z) e^{i\ell_2 \theta} e^{-2i\omega t}], \quad (4b)$$

each of which satisfies separate orbital and spin invariance properties

$$R(\gamma\alpha)\mathbf{F}_1(\mathbf{r}, t) = \mathbf{F}_1(\mathbf{r}, t + \gamma\alpha/\omega), \quad (5a)$$

$$\mathbf{F}_1(R^{-1}(\alpha)\mathbf{r}, t) = \mathbf{F}_1(\mathbf{r}, t + \ell_1\alpha/\omega), \quad (5b)$$

$$R(\gamma\alpha)\mathbf{F}_2(\mathbf{r}, t) = \mathbf{F}_2(\mathbf{r}, t - \gamma\alpha/2\omega), \quad (5c)$$

$$\mathbf{F}_2(R^{-1}(\alpha)\mathbf{r}, t) = \mathbf{F}_2(\mathbf{r}, t + \ell_2\alpha/2\omega). \quad (5d)$$

The correct CR invariance of the system can then be found by requiring that the combined time delay imposed by Eqs. (5a, 5b) matches that produced by the combination of Eqs. (5c, 5d), so that

$$\frac{\ell_1\alpha}{\omega} + \frac{\gamma\alpha}{\omega} = \frac{\ell_2\alpha}{2\omega} - \frac{\gamma\alpha}{2\omega} \implies \gamma = \frac{\ell_2 - 2\ell_1}{3}, \quad (6)$$

with a time-delay constant $\tau = \frac{\ell_1 + \ell_2}{3\omega}$. This then sets the TKAM charge $j_\gamma^{(n)}$ for each driver, defined in analogy to the OAM charge in Eqs. (5b, 5d) by requiring that

$$R(\gamma\alpha)\mathbf{F}_n(R^{-1}(\alpha)\mathbf{r}, t) = \mathbf{F}(\mathbf{r}, t + j_\gamma^{(n)}\alpha/n\omega), \quad (7)$$

to be $j_\gamma^{(n)} = n\omega\tau$ [43].

Turning to the HHG radiation, we can now see the conserved TKAM charge in action, via the standard correspondence between dynamical symmetries and conserved charges, and their associated selection rules [44, 45]. Since in our configuration the application of a CR to the driving field is equivalent to a time delay, via Eq. (2), and the gaseous generating medium is unaffected by the transformation, the same must be true for the emitted HHG radiation. With the XUV emission's TKAM charge defined as in Eq. (7), the CR invariance then guarantees the conservation of the TKAM charge as expressed in Eq. (1).

To explore the conservation of TKAM in HHG, we perform numerical simulations of HHG in the configuration shown in Fig. 1 by solving the Schrödinger-Maxwell equations for a sample of atoms in the interaction region within the SFA+ approximation and using the electromagnetic field propagator described in Ref. 46; further details of our method can be found in Refs. 15, 17, 47.

We consider the harmonic emission driven by a bicircular field with $\ell_1 = \ell_2 = 1$, equal beam waists of $30\text{ }\mu\text{m}$, pulses of total intensity $I = 2 \times 10^{14}\text{ W/cm}^2$. The ω and 2ω driving pulse envelopes are modelled as a trapezoidal function with 5.3 fs of linear turn-on, 10.7 fs of constant amplitude and 5.3 fs of linear turn-off. High-order harmonics are generated in a thin slab argon gas jet and propagated to the far-field (i.e. longitudinal phase-matching effects are neglected, since in OAM-HHG the transverse phase-matching effects dominate, as demonstrated in Refs. 17 and 47).

We present our results in Fig. 2, by comparing the (a) OAM and (b) TKAM spectra of the circularly polarized components of the HHG emission (shown in red and blue, respectively), as a function of harmonic order. Here the conservation law is clear in the linear trend observed in the TKAM spectrum, which embodies its form from Eq. (1). A similar conservation law can also be observed for HHG driven by the monochromatic CR-invariant beams produced by conical refraction, with $\gamma = 1/2$ [48].

To examine the harmonic emission more closely, we turn to its structure in the time domain. In HHG driven by OAM beams, where a spatial rotation induces a time delay in the driver, the attosecond pulse train (APT) will be naturally shaped as a spiral [15, 18, 47]. In CR-invariant beams, where spatial rotations are also associated with time delays on the driver, a similar spiral appears, with an additional polarization-twist structure caused by the polarization component of the invariance property [48]. We present this in Fig. 3(a), using an isosurface plot for the XUV intensity and the color scale to represent the polarization direction, which twists smoothly along the attosecond pulse spiral.

To study this polarization structure quantitatively, we require a measure of the absolute orientation of the APT at different azimuthal points in the beam—and, ideally,

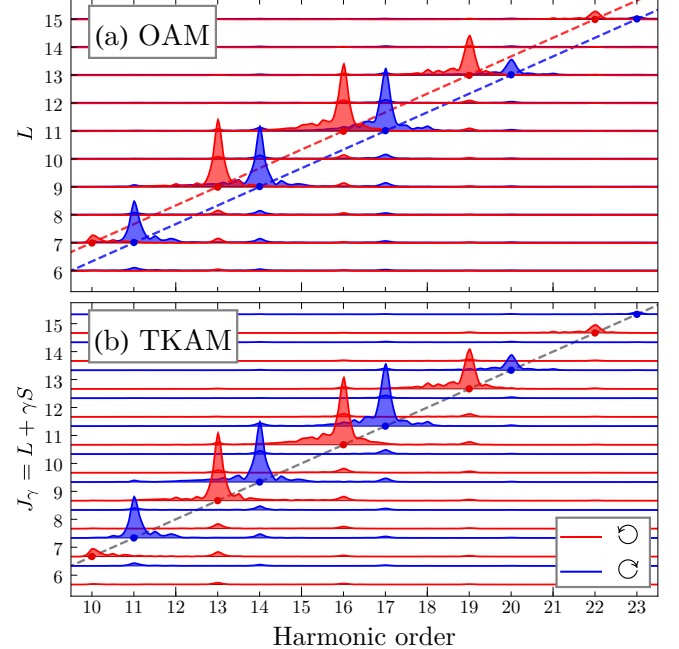


FIG. 2. Simulated HHG spectra of the right and left-polarized components (shown in red and blue, respectively) driven by a bicircular field with $\ell_1 = \ell_2 = 1$. We compare the (a) OAM and (b) TKAM spectra, with $\gamma = -1/3$, as a function of the harmonic order. We calculate the OAM spectrum by taking a standard Fourier series over the azimuthal dependence and integrating over the radial dependence. For the TKAM spectrum the OAM charge of the \circlearrowleft - and \circlearrowright -polarized components is shifted by γ times their SAM. The conservation of TKAM is clear in the linear trend shown in (b).

an orientation measure that is sensitive to the pulse train's structure as a sequence of linearly-polarized pulses at an angle to each other [35, 38]. For monochromatic radiation, the polarization ellipse orientation angle is obtained via the eigenvectors of the polarization matrix $\langle E_i E_j \rangle$ [49], which can be expressed more cleanly as the phase of the quadrupole component $T_{22} = \int_{-\infty}^{\infty} (E_x(t) + iE_y(t))^2 dt$ of that second field moment [33]. The symmetry of our APT means that the average orientation is undefined, so we turn to the time-dependent analysis toolkit of strong-field science (specifically, the Gabor transform [50]) to modify it to a time-windowed version,

$$T_{22}(\mathbf{r}, t) = \int_{-\infty}^{\infty} (E_x^{(\text{xuv})}(\mathbf{r}, t') + iE_y^{(\text{xuv})}(\mathbf{r}, t'))^2 \times e^{-(t'-t)^2/2\sigma^2} dt' \quad (8)$$

from which the local polarization-ellipse orientation angle can be obtained as $\frac{1}{2} \arg(T_{22}(\mathbf{r}, t))$ [51]. Thus, for example, a linearly polarized pulse along $\hat{\mathbf{e}}_x$ produces a positive T_{22} , an $\hat{\mathbf{e}}_y$ polarization gives a negative moment, and there is a continuous passage between the two behaviours.

The time-windowed quadrupole moment, which we plot in Fig. 3(b), clearly shows the twisted-spiral structure of the XUV emission: the amplitude is constrained to two strips that wind around the azimuthal axis, acquiring a time delay of $4\pi/3\omega$ after one revolution, while the polarization direction, indicated by the hue color scale, turns by -120° over that span, in an essentially linear progression. This directly confirms the CR invariance of

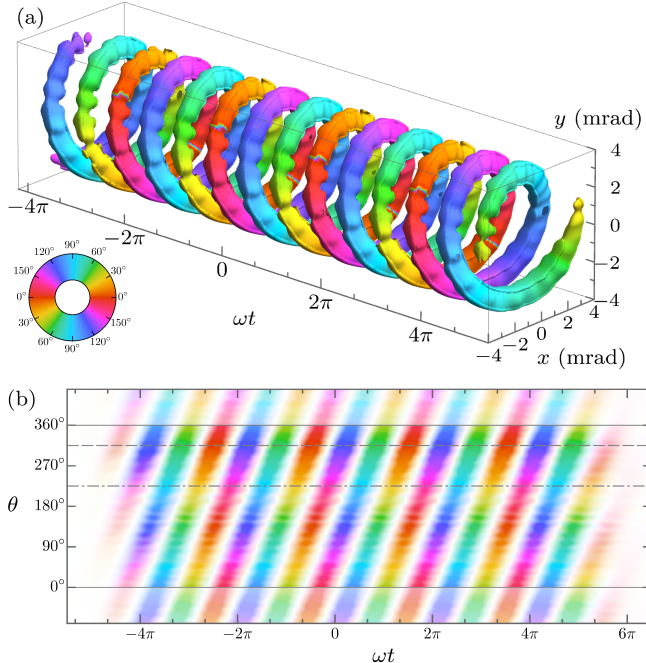


FIG. 3. Twisted-spiral structure of the attosecond pulse train emitted by CR-invariant bicircular drivers at $\ell_1 = \ell_2 = 1$, as in Fig. 2. (a) Iso-intensity surface of the HHG emission, filtered above harmonic order 10, over the far-field divergence Cartesian coordinates x and y , with the color denoting the local polarization direction as in (b). (b) Polarization angle of the attosecond pulses over azimuthal emission angle θ , obtained from the time-windowed $T_{22}(\mathbf{r}, t)$ field moment of Eq. (8) with $\sigma = 15^\circ/\omega$ and integrated over angular divergence, with $\frac{1}{2}\arg(T_{22}(\mathbf{r}, t))$ plotted as the hue and $|T_{22}(\mathbf{r}, t)|$ (which closely follows the XUV intensity) as the color saturation. The polarization angle rotates by -120° over each turn of the spiral, directly confirming the $\gamma = -1/3$ rotation-coordination parameter of the beam. At each fixed θ , the polarization jumps over three complementary colors such as blue-green-red (dashed line) or cyan-yellow-magenta (dot-dashed line), showing the local polarization structure as a train of linear pulses at 120° from each other.

the HHG emission, in the sense of Eq. (2), and, with that, its nontrivial torus-knot topology.

Here it is also instructive to broaden our scope to consider what happens when the coordinated-rotation invariance gets broken, by perturbing the OAM of one or both of the drivers. For single-color driving fields, this fully brings into play the nonperturbative physics of HHG, through the intrinsic dipole phase of the harmonics, which is proportional to the field intensity and depends on the quantum path followed in the HHG process [52–55]. In that case, an OAM perturbation imprints an azimuthal intensity gradient, which, through the intrinsic phase, broadens the OAM content of each harmonic [17].

With bicircular drivers, on the other hand, we can take advantage of the two-field configuration to perform a wider exploration of the nonperturbative physics of OAM-HHG. One way that this can be done is by using an OAM perturbation to imprint an azimuthal intensity gradient, as in the one-color case. We showcase this in Fig. 4(b), where we divert 10% of the intensity to a donut-like $\ell = 0$ mode on both drivers with an $r^2 e^{-r^2/\sigma^2}$

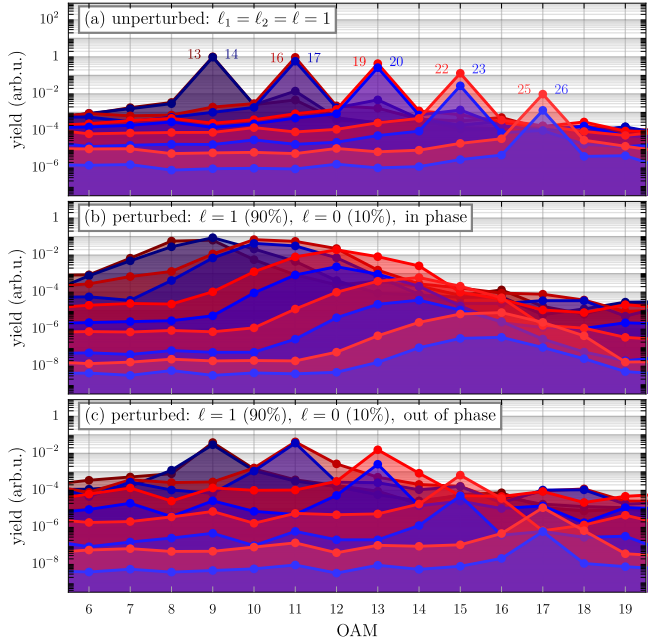


FIG. 4. OAM spectrum of the HHG radiation driven by a bicircular field with $\ell_1 = \ell_2 = 1$ (a), as in Fig. 2, as well as with a 10% intensity perturbation on a donut-like $\ell = 0$ mode on both drivers: (b) with both perturbations in phase, so the intensity profiles match, and (c) with the perturbations in opposite phase, so the intensity profiles are complementary. (The lines are color-coded by the harmonic order, as labelled in (a).) We can identify the OAM broadening as a consequence of an azimuthal intensity gradient (b) and different quantum path dynamics (c).

amplitude profile; as in the one-color case [17], the OAM and TKAM spectra of each harmonic is broadened. Alternatively, one can also imprint complementary intensity profiles to the two fields, by switching the relative phase of one of the OAM $\ell = 0$ donut-like modes, so that the total intensity is constant but the intensity ratio $I_\omega/I_{2\omega}$ varies around the beam. This still affects the harmonic emission, broadening the OAM spectrum as shown in Fig. 4(c), but the mechanism is different: here the quantum phase is constant, but the intensity ratio affects the quantum-path dynamics [40], which alters both the semiclassical quantum-path dynamics and the vector aspects of the recollision [39]. We thus demonstrate that the dominant contribution to OAM broadening comes from the azimuthal intensity gradient (i.e. with both perturbations in phase), which further reinforces the requirement of clean OAM driver modes to obtain single-OAM-mode harmonics.

Finally, it is important to note that, in addition to the demonstration of the TKAM conservation law, this configuration also allows for the production of XUV radiation with controllable OAM, as recently pointed out in Refs. 56, 57. The existing collinear experiments [16–18] are invariant under spatial rotations, so that OAM is conserved and scales linearly, with the q th harmonic carrying OAM $\ell_q = q\ell$ [15, 17]. For high q , this OAM is often too big to be useful in applications, and it is challenging to detect and characterize in the first place [16, 58]. This problem can be fixed by using a non-collinear perturbation on the driver [16, 19, 20], but that

comes at the price that the harmonic yield is spread over a range of different OAM modes.

On the other hand, the use of CR-invariant drivers allows us to imprint the q^{th} harmonic with an arbitrary OAM ℓ_q by, in effect, leveraging the bicircular spin selection rules [22, 24, 44] to concentrate all of the harmonic yield at a given harmonic order into a single OAM

mode. Thus, this configuration provides a source of bright XUV radiation with circular polarization and controllable OAM, which can be used to explore spin-orbit coupling in light, molecules and materials [59], for high-contrast high-resolution spiral-phase imaging [60] of magnetic domains [61], super-resolution XUV microscopy [16] and lithography [62], mechanical manipulation of matter, as well as a number of spectroscopic applications [63, 64].

-
- [1] R. BOYD. *Nonlinear optics* (Academic Press, San Diego, 2003).
- [2] D. E. NEUENSCHWANDER. *Emmy Noether's Wonderful Theorem* (John Hopkins University Press, Baltimore, 2011).
- [3] N. BLOEMBERGEN. Conservation laws in nonlinear optics. *J. Opt. Soc. Am.* **70** no. 12, pp. 1429–1436 (1980).
- [4] G. MOLINA-TERRIZA, J. P. TORRES AND L. TORNER. Twisted photons. *Nature Phys.* **3** no. 5, pp. 305–310 (2007).
- [5] J. COURTIAL et al. Second-harmonic generation and the conservation of orbital angular momentum with high-order laguerre-gaussian modes. *Phys. Rev. A* **56** no. 5, pp. 4193–4196 (1997).
- [6] M. IVANOV AND O. SMIRNOVA. Multielectron high harmonic generation: simple man on a complex plane. In T. SCHULTZ AND M. VRAKKING (eds.), *Attosecond and XUV Physics: Ultrafast Dynamics and Spectroscopy*, pp. 201–256 (Wiley-VCH, Weinheim, 2014). arXiv: 1304.2413.
- [7] F. KRAUSZ AND M. IVANOV. Attosecond physics. *Rev. Mod. Phys.* **81** no. 1, pp. 163–234 (2009).
- [8] T. POPMINTCHEV et al. Bright coherent ultrahigh harmonics in the keV X-ray regime from mid-infrared femtosecond lasers. *Science* **336** no. 6086, pp. 1287–1291 (2012). JILA e-print.
- [9] M. LEWENSTEIN et al. Theory of high-harmonic generation by low-frequency laser fields. *Phys. Rev. A* **49** no. 3, pp. 2117–2132 (1994).
- [10] P. B. CORKUM. Plasma perspective on strong field multiphoton ionization. *Phys. Rev. Lett.* **71** no. 13, pp. 1994–1997 (1993).
- [11] K. J. SCHAFER et al. Above threshold ionization beyond the high harmonic cutoff. *Phys. Rev. Lett.* **70** no. 11, pp. 1599–1602 (1993).
- [12] M. D. PERRY AND J. K. CRANE. High-order harmonic emission from mixed fields. *Phys. Rev. A* **48** no. 6, pp. R4051–R4054 (1993).
- [13] J. B. BERTRAND et al. Ultrahigh-order wave mixing in noncollinear high harmonic generation. *Phys. Rev. Lett.* **106** no. 2, p. 023001 (2011).
- [14] M. ZÜRCH et al. Strong-field physics with singular light beams. *Nature Phys.* **8** no. 10, pp. 743–746 (2012).
- [15] C. HERNÁNDEZ-GARCÍA et al. Attosecond extreme ultraviolet vortices from high-order harmonic generation. *Phys. Rev. Lett.* **111** no. 8, p. 083602 (2013). arXiv:1507.00635.
- [16] G. GARIEPY et al. Creating high-harmonic beams with controlled orbital angular momentum. *Phys. Rev. Lett.* **113** no. 15, p. 153901 (2014).
- [17] L. REGO et al. Nonperturbative twist in the generation of extreme-ultraviolet vortex beams. *Phys. Rev. Lett.* **117** no. 16, p. 163202 (2016).
- [18] R. GÉNEAUX et al. Synthesis and characterization of attosecond light vortices in the extreme ultraviolet. *Nature Commun.* **7**, p. 12583 (2016). OSU eprint.
- [19] F. KONG et al. Controlling the orbital angular momentum of high harmonic vortices. *Nature Commun.* **8**, p. 14970 (2017).
- [20] D. GAUTHIER et al. Tunable orbital angular momentum in high-harmonic generation. *Nature Commun.* **8**, p. 14971 (2017).
- [21] C. HERNÁNDEZ-GARCÍA. High harmonic generation: A twist in coherent x-rays. *Nature Phys.* **13** no. 4, p. 327 (2017).
- [22] A. FLEISCHER et al. Spin angular momentum and tunable polarization in high-harmonic generation. *Nature Photon.* **8** no. 7, pp. 543–549 (2014). arXiv:1310.1206.
- [23] M. IVANOV AND E. PISANTY. High-harmonic generation: taking control of polarization. *Nature Photon.* **8** no. 7, pp. 501–503 (2014). Imperial College eprint.
- [24] E. PISANTY, S. SUKIASYAN AND M. IVANOV. Spin conservation in high-order-harmonic generation using bicircular fields. *Phys. Rev. A* **90** no. 4, p. 043829 (2014). arXiv:1404.6242.
- [25] D. D. HICKSTEIN et al. Non-collinear generation of angularly isolated circularly polarized high harmonics. *Nature Photon.* **9** no. 11, pp. 743 – 750 (2015). JILA eprint.
- [26] P.-C. HUANG et al. Polarization control of isolated high-harmonic pulses. *Nature Photon.* **12** no. 6, p. 349 (2018). JILA eprint.
- [27] J. LEACH et al. Interferometric methods to measure orbital and spin, or the total angular momentum of a single photon. *Phys. Rev. Lett.* **92** no. 1, p. 013601 (2004).
- [28] K. E. BALLANTINE, J. F. DONEGAN AND P. R. EASTHAM. There are many ways to spin a photon: Half-quantization of a total optical angular momentum. *Sci. Adv.* **2** no. 4, p. e1501748 (2016).
- [29] M. R. DENNIS. Polarization singularities in paraxial vector fields: morphology and statistics. *Opt. Commun.* **213** no. 4–6, pp. 201–221 (2002). Southampton eprint.
- [30] I. FREUND. Cones, spirals, and Möbius strips, in elliptically polarized light. *Opt. Commun.* **249** no. 1–3, pp. 7–22 (2005).
- [31] T. BAUER et al. Observation of optical polarization Möbius strips. *Science* **347** no. 6225, pp. 964–966 (2015). Rochester U eprint.
- [32] T. BAUER et al. Optical polarization Möbius strips and points of purely transverse spin density. *Phys. Rev. Lett.* **117** no. 1, p. 013601 (2016). arXiv:1601.06072.
- [33] E. PISANTY et al. Knotting fractional-order knots with the polarization state of light (2018). arXiv:1808.05193.
- [34] H. EICHMANN et al. Polarization-dependent high-order two-color mixing. *Phys. Rev. A* **51** no. 5, pp. R3414–R3417 (1995).
- [35] D. B. MILOŠEVIĆ AND W. BECKER. Attosecond pulse trains with unusual nonlinear polarization. *Phys. Rev. A* **62** no. 1, p. 011403 (2000).
- [36] O. KFIR et al. Generation of bright phase-matched circularly-polarized extreme ultraviolet high harmonics.

- Nature Photon.* **9** no. 2, p. 99 (2015). arXiv:1401.4101.
- [37] T. FAN et al. Bright circularly polarized soft x-ray high harmonics for x-ray magnetic circular dichroism. *Proc. Natl. Acad. Sci. USA* **112** no. 46, pp. 14 206–14 211 (2015).
- [38] C. CHEN et al. Tomographic reconstruction of circularly polarized high-harmonic fields: 3D attosecond metrology. *Sci. Adv.* **2** no. 2, p. e1501333 (2016).
- [39] E. PISANTY AND A. JIMÉNEZ-GALÁN. Strong-field approximation in a rotating frame: High-order harmonic emission from p states in bicircular fields. *Phys. Rev. A* **96** no. 6, p. 063 401 (2017). arXiv:1709.00397.
- [40] A. JIMÉNEZ-GALÁN et al. Control of attosecond light polarization in two-color bicircular fields. *Phys. Rev. A* **97** no. 2, p. 023 409 (2018). arXiv:1805.02250.
- [41] C. C. ADAMS. *The Knot Book: An elementary introduction to the mathematical theory of knots* (American Mathematical Society, Providence, Rhode Island, 2004).
- [42] Irrational coordination parameters are also achievable, using combinations of non-commensurate bichromatic drivers and, thus, a quasi-periodic driving field. While possible, quasi-periodic fields require infinite time and infinitely small bandwidth to distinguish from nearby commensurate frequency pairs, a requirement that is generally at odds with physical experiments and particularly so with the short pulses required by HHG.
- [43] This formalism extends naturally to bicircular combinations of frequencies $p\omega$ and $q\omega$, with p, q coprime integers, for which $\gamma = \frac{p\ell_1 - q\ell_2}{p+q}$ and $\tau = \frac{\ell_1 + \ell_2}{(p+q)\omega}$.
- [44] O. E. ALON, V. AVERBUKH AND N. MOISEYEV. Selection rules for the high harmonic generation spectra. *Phys. Rev. Lett.* **80** no. 17, pp. 3743–3746 (1998).
- [45] V. AVERBUKH, O. E. ALON AND N. MOISEYEV. Stability and instability of dipole selection rules for atomic high-order-harmonic-generation spectra in two-beam setups. *Phys. Rev. A* **65** no. 6, p. 063 402 (2002).
- [46] C. HERNÁNDEZ-GARCÍA et al. High-order harmonic propagation in gases within the discrete dipole approximation. *Phys. Rev. A* **82** no. 3, p. 033 432 (2010).
- [47] C. HERNÁNDEZ-GARCÍA et al. Quantum-path signatures in attosecond helical beams driven by optical vortices. *New J. Phys.* **17** no. 9, p. 093 029 (2015).
- [48] A. TURPIN et al. Extreme ultraviolet fractional orbital angular momentum beams from high harmonic generation. *Sci. Rep.* **7**, p. 43 888 (2017).
- [49] I. FREUND. Coherency matrix description of optical polarization singularities. *J. Opt. A: Pure Appl. Opt.* **6** no. 5, p. S229 (2004).
- [50] P. ANTOINE, B. PIRAX AND A. MAQUET. Time profile of harmonics generated by a single atom in a strong electromagnetic field. *Phys. Rev. A* **51** no. 3, pp. R1750–R1753 (1995).
- [51] For the TKAM beams we use to drive the emission, the knotted structure of the beam is best explored through the third field moment $\langle E_i E_j E_k \rangle$, and more specifically its hexapolar component $T_{33}(\mathbf{r}) = \int_{-\infty}^{\infty} (E_x(\mathbf{r}, t) + iE_y(\mathbf{r}, t))^3 dt$, which intrinsically respects the three-fold rotational symmetry of the polarization [33]. For a broadband APT, however, this is not a suitable measure, since its spectral characteristics favour contributions from low-order harmonics, so that it acquires an unphysical dependence on the filter used to isolate the pulse train from the perturbative response at low harmonic orders.
- [52] A. L'HUILLIER et al. Calculations of high-order harmonic-generation processes in xenon at 1064 nm. *Phys. Rev. A* **46** no. 5, pp. 2778–2790 (1992).
- [53] M. LEWENSTEIN, P. SALIÈRES AND A. L'HUILLIER. Phase of the atomic polarization in high-order harmonic generation. *Phys. Rev. A* **52** no. 6, pp. 4747–4754 (1995). LU eprint.
- [54] A. ZAÏR et al. Quantum path interferences in high-order harmonic generation. *Phys. Rev. Lett.* **100** no. 14, p. 143 902 (2008). ETH eprint.
- [55] C. HERNÁNDEZ-GARCÍA AND L. PLAJA. Off-axis compensation of attosecond pulse chirp. *J. Phys. B: At. Mol. Opt. Phys.* **45** no. 7, p. 074 021 (2012).
- [56] W. PAUFLER, B. BÖNING AND S. FRITZSCHE. Tailored orbital angular momentum in high-order harmonic generation with bicircular Laguerre-Gaussian beams. *Phys. Rev. A* **98** no. 1, p. 011 401 (2018).
- [57] K. M. DORNEY et al. Helicity in a twist: Controlling the polarization, divergence and vortex charge of attosecond high-harmonic beams via simultaneous spin-orbit momentum conservation. *Nature Photon.* In press (2018).
- [58] F. SANSON et al. Hartmann wavefront sensor characterization of a high charge vortex beam in the extreme ultraviolet spectral range. *Opt. Lett.* **43** no. 12, pp. 2780–2783 (2018).
- [59] F. CARDANO AND L. MARRUCCI. Spin-orbit photonics. *Nature Photon.* **9** no. 12, pp. 776–778 (2015).
- [60] S. FÜRHAPTER et al. Spiral phase contrast imaging in microscopy. *Opt. Express* **13** no. 3, pp. 689–694 (2005).
- [61] O. KFIR et al. Nanoscale magnetic imaging using circularly polarized high-harmonic radiation. *Sci. Adv.* **3** no. 12, p. eaao4641 (2017).
- [62] T. F. SCOTT et al. Two-color single-photon photoinitiation and photoinhibition for subdiffraction photolithography. *Science* **324** no. 5929, pp. 913–917 (2009). CU eprint.
- [63] P. REBERNIK RIBIĆ et al. Extreme-ultraviolet vortices from a free-electron laser. *Phys. Rev. X* **7** no. 3, p. 031 036 (2017).
- [64] C. HERNÁNDEZ-GARCÍA et al. Generation and applications of extreme-ultraviolet vortices. *Photonics* **4** no. 2, p. 28 (2017).

Acknowledgements

E.P. acknowledges Cellex-ICFO-MPQ fellowship funding; E.P. and M.L. acknowledge the Spanish Ministry MINECO (National Plan 15 Grant: FISICATEAMO No. FIS2016-79508-P, SEVERO OCHOA No. SEV-2015-0522, FPI), European Social Fund, Fundació Cellex, Generalitat de Catalunya (AGAUR Grant No. 2017 SGR 1341 and CERCA/Program), ERC AdG OSYRIS, EU FETPRO QUIC, and the National Science Centre, Poland-Symfonia Grant No. 2016/20/W/ST4/00314. A.P. acknowledges funding from Comunidad de Madrid through TALENTO grant ref. 2017-T1/IND-5432. J.S.R., L.P. and C.H.-G. acknowledge support from Junta de Castilla y León (SA046U16) and Ministerio de Economía y Competitividad (FIS2013-44174-P, FIS2016-75652-P). C.H.-G. acknowledges support from a 2017 Leonardo Grant for Researchers and Cultural Creators, BBVA Foundation. L.R. acknowledges support from Ministerio de Educación, Cultura y Deporte (FPU16/02591). We thankfully acknowledge the computer resources at MareNostrum and the technical support provided by Barcelona Supercomputing Center (RES-AECT-2014-2-0085). This research made use of the high-performance computing resources of the Castilla y León Supercomputing Center (SCAYLE, www.scayle.es), financed by the European Regional Development Fund (ERDF).